

## Bulk band dispersion in $\text{Ti}_2\text{O}_3$ and $\text{V}_2\text{O}_3$

Kevin E. Smith\* and Victor E. Henrich

*Applied Physics, Yale University, 15 Prospect Street, New Haven, Connecticut 06520*

(Received 4 December 1987)

We report here a comprehensive study of the bulk electronic structure of single-crystal  $\text{Ti}_2\text{O}_3$  and  $\text{V}_2\text{O}_3$  using both angle-integrated and angle-resolved photoemission and synchrotron radiation. The electronic structure of these materials is of particular interest because of the metal-insulator transitions which they undergo. Slight ( $< 0.4$  eV) dispersion of the cation  $3d$  bands is observed in both materials, supporting a band model for their electronic structure. Large discrepancies are observed between the measured band dispersion and published calculations for both materials. The O  $2p$  emission is too broad to permit extraction of unambiguous band dispersions. Resonant photoemission is observed from cation  $3d$  states in both  $\text{Ti}_2\text{O}_3$  and  $\text{V}_2\text{O}_3$  as the photon energy is swept through the cation  $3p \rightarrow 3d$  optical-absorption edge. A valence-band satellite is resolved in the angle-integrated photoemission spectra from  $\text{V}_2\text{O}_3$ ; resolving this feature shows that the actual width of the O  $2p$  band in  $\text{V}_2\text{O}_3$  is almost 2.5 eV narrower than previous studies indicated.

### I. INTRODUCTION

The bulk electronic structure of  $\text{Ti}_2\text{O}_3$  and  $\text{V}_2\text{O}_3$  has been the object of much experimental and theoretical investigation over the past 40 years. The interest in these materials comes primarily from a desire to understand the nature of the metal-insulator transitions which these materials undergo, although even the nature of the room-temperature metallic state in  $\text{V}_2\text{O}_3$  is controversial.<sup>1-10</sup> A variety of experimental tools have been used to probe the electronic structure of these materials,<sup>1</sup> and, with the advent of photoemission spectroscopy as a powerful method of extracting electronic-structure information, both materials have been the subject of numerous photoemission studies.<sup>11-20</sup> Unfortunately, the majority of these studies suffer from either using powdered samples<sup>16-18</sup> (as opposed to single crystals), which allows the metal cations to have a variety of ligand coordinations, or by using single crystals whose surfaces are either damaged (i.e., have a high defect density induced by inert-gas ion bombardment)<sup>14,15</sup> or are heavily oxidized.<sup>19,20</sup> Recently, however, there have been a number of studies<sup>11-13</sup> that have used single crystals cleaved in ultrahigh vacuum (UHV) and that have taken care to avoid both contamination and defects. While these angle-integrated photoemission studies allowed for the determination of the bulk density of states, they did not allow energy-band dispersions to be measured.

We present here a comprehensive angle-resolved ultraviolet-photoemission-spectroscopy (ARUPS) study, using synchrotron radiation, of single-crystal  $\text{Ti}_2\text{O}_3$  and  $\text{V}_2\text{O}_3$ . By using this technique we have, for the first time, mapped out the  $d$ -band dispersion of these materials and tested the validity of the available band-structure calculations.<sup>2,10</sup> We also present angle-integrated photoemission spectra for  $\text{V}_2\text{O}_3$  taken using synchrotron radiation and report one of the first observations of resonant photoemission in a vanadium oxide; discussion of the details of

resonant photoemission in these oxides is presented elsewhere.<sup>21</sup>

In Sec. II we present a review of the current experimental and theoretical understanding of the electronic structure of  $\text{Ti}_2\text{O}_3$  and  $\text{V}_2\text{O}_3$ . Section III contains a brief review of the theories of ARUPS and resonant photoemission and discusses some calculations relevant to ARUPS studies of cleaved  $\text{Ti}_2\text{O}_3$  and  $\text{V}_2\text{O}_3$ . Section IV describes the experimental methods and sample-preparation techniques. The photoemission data obtained for both materials are presented in Sec. V, and Sec. VI discusses our results in reference to the available theoretical calculations. The paper concludes with a summary of results in Sec. VII.

### II. $\text{Ti}_2\text{O}_3$ AND $\text{V}_2\text{O}_3$ : A REVIEW OF ELECTRONIC-STRUCTURE THEORIES

#### A. General considerations

Both  $\text{Ti}_2\text{O}_3$  and  $\text{V}_2\text{O}_3$  have the corundum structure with a trigonal (rhombohedral) Bravais lattice. The unit cell (see, for example, Refs. 1-3) consists of a ten-atom basis set made up of two  $M_2\text{O}_3$  molecular units. The crystal field splits the atomic  $d$  states into a pair of  $e^\sigma$  orbitals, a pair of  $e_g^\pi$  orbitals, and an  $a_{1g}$  orbital.<sup>1</sup> The  $a_{1g}$  orbital is directed along the hexagonal  $c$  axis, forming a covalent molecular bond between pairs of metal ions,<sup>3</sup> the  $e_g^\pi$  orbitals are involved in bonding between metal ions in the basal plane, and the  $e_g^\sigma$  orbitals are directed towards nearest-neighbor oxygen atoms. The ordering of these orbitals in energy is different for  $\text{Ti}_2\text{O}_3$  and  $\text{V}_2\text{O}_3$  (see Fig. 1) and will be discussed below. The  $a_{1g}$  band can contain up to one electron per metal atom (i.e., two electrons per molecular unit, or four electrons per unit cell). The  $e_g^\pi$  and  $e_g^{\pi*}$  bands, which overlap, can contain up to four electrons per metal atom (the asterisk indicates an antibonding orbital). The remaining  $e^\sigma$ ,  $e^{\sigma*}$ , and  $a_{1g}^*$

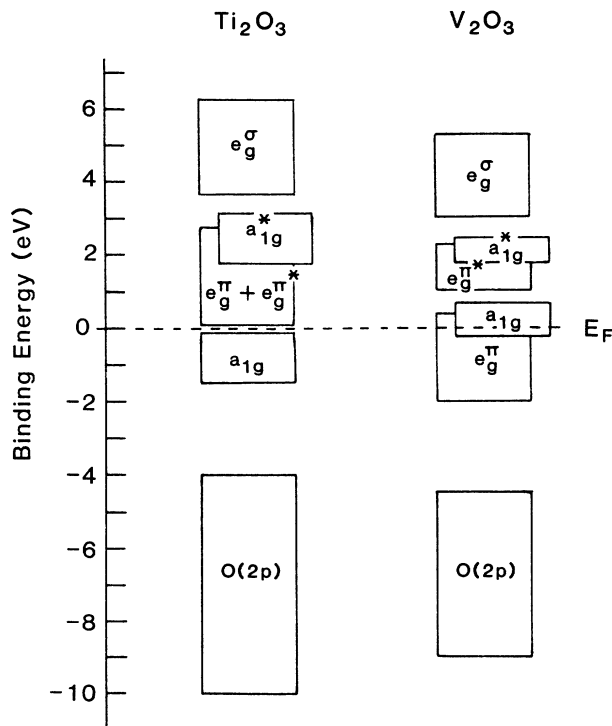


FIG. 1. Empirical band structures for  $\text{Ti}_2\text{O}_3$  and  $\text{V}_2\text{O}_3$  (from Ref. 1).

bands can together hold five electrons per metal atom. Occupation of the  $a_{1g}$  band decreases the  $c/a$  ratio by increasing the metal-metal pair bonding in the  $c$  direction; conversely, occupation of the  $e_g^\pi$  states increases the  $c/a$  ratio.

### B. $\text{Ti}_2\text{O}_3$

Below about  $200^\circ\text{C}$ ,  $\text{Ti}_2\text{O}_3$  is a narrow-band-gap semiconductor ( $E_{\text{gap}} < 0.1$  eV).<sup>1,22</sup> The order of the bands, as shown in Fig. 1, was determined primarily from optical measurements.<sup>23</sup> Angle-integrated photoemission spectra have confirmed the width and position of the bands.<sup>12,13</sup> At these temperatures, the  $a_{1g}$  band is filled, giving  $\text{Ti}_2\text{O}_3$  a  $3d^1$  electronic configuration. As is shown in Fig. 1, this material derives its semiconducting nature from the existence of the gap between this filled  $a_{1g}$  band and the unoccupied  $e_g^\pi$  band. Above  $200^\circ\text{C}$ , the material goes through a broad ( $\approx 200^\circ\text{C}$  wide) semiconductor-to-metal transition with an accompanying increase in  $c/a$  ratio but no change in symmetry.<sup>24,25</sup> Although less controversial than the transition in  $\text{V}_2\text{O}_3$ , the exact nature of this transition is unclear.<sup>1,8</sup> A band-structure calculation that includes intra-atomic Coulomb interactions (which must be considered in  $\text{Ti}_2\text{O}_3$  since  $U$ , the intra-atomic Coulomb potential between  $d$  electrons, is comparable in magnitude to  $W$ , the electronic bandwidth) seems to predict many of the observed phenomena.<sup>10</sup>

### C. $\text{V}_2\text{O}_3$

$\text{V}_2\text{O}_3$  undergoes a first-order transition at 150 K from a monoclinic antiferromagnetic insulator at low tempera-

tures to a trigonal metallic state. In addition, above about  $450\text{--}500$  K there is a broad ( $\approx 150$  K) second-order transition from the metallic state to a semiconducting one; this transition is similar to that in  $\text{Ti}_2\text{O}_3$ . There is a vast body of literature devoted to the nature of these transitions (see Refs. 1, 4–7, 10, and references therein). More relevant to our experiments, which probe the nature of the room-temperature metallic state, are theories of the electronic structure of this state itself. The metallic phase displays a variety of anomalous properties, among them an extremely large  $T^2$  term in the electrical resistivity ( $10^3$  times larger than in transition metals),<sup>26</sup> and a very large electronic specific heat.<sup>27</sup> Central to understanding  $\text{V}_2\text{O}_3$ , and the differences between it and  $\text{Ti}_2\text{O}_3$ , is the realization that it possesses two types of  $3d$  electrons; with a  $3d^2$  configuration, both the  $a_{1g}$  and  $e_g^\pi$  bands are partially populated (see Fig. 1). As in  $\text{Ti}_2\text{O}_3$ , the order of these bands in energy has been determined from optical experiments,<sup>28</sup> but the width and separation of the bands have not been unambiguously determined; this will be discussed in Sec. VI. The most comprehensive theory of the metallic state assumes a Hubbard model and has the  $a_{1g}$  orbital half full, with 0.5 electrons per V atom contained within it and the remaining 1.5 electrons per V atom residing in the  $e_g^\pi$  band.<sup>3</sup> The Fermi level lies within both bands, but the thermodynamic and transport properties of metallic  $\text{V}_2\text{O}_3$  are postulated to be determined primarily by the  $e_g^\pi$  electrons.

## III. ARUPS AND RESONANT PHOTOEMISSION: THEORY

### A. ARUPS

#### 1. General

The technique of angle-resolved photoemission, when used in conjunction with a tunable ultraviolet photon source (i.e., synchrotron radiation), is the most powerful method available for fully mapping out the dispersion of electrons inside a crystal.<sup>29,30</sup> The technique was initially used to study single crystals of simple metals (see, for example, Refs. 30–38) and has been successfully used to examine the band structure of elemental<sup>39</sup> and compound semiconductors<sup>40</sup> as well as metal carbides, nitrides, and sulfides.<sup>41–46</sup> However, the energy-band dispersions of electrons in metal oxides have been less widely studied. Among the oxides studied prior to this work are  $\text{ZnO}$ ,<sup>47,48</sup>  $\text{SrTiO}_3$ ,<sup>49</sup> and  $\text{Fe}_3\text{O}_4$ .<sup>50,51</sup> The reasons for the dearth of information on oxides are many, ranging from the difficulty of obtaining suitable single crystals to the difficulty in interpreting the spectra since, in comparison to metals, the photoemission features tend to be quite broad. As will be seen in Sec. V, the experimentally observed  $d$ -band emission in  $\text{Ti}_2\text{O}_3$  and  $\text{V}_2\text{O}_3$  is narrow enough to observe band dispersions clearly, but the emission from the oxygen  $2p$  band exhibits much broader structures, making it harder to identify specific dispersions (although gross motion of the bands can be observed).  $\text{Ti}_2\text{O}_3$  is an ideal oxide upon which to test the applicability of ARUPS to this class of materials; its

semiconducting nature eliminates any surface charging effects, and the Ti 3*d* emission is well separated from the O 2*p* emission, allowing for unambiguous interpretation of the *d*-band dispersion.

## 2. Theory

The theory supporting the use of angle-resolved photoemission to measure energy-band dispersions in solids is well established and has been reviewed in a number of publications.<sup>29,30,36,41,42,52</sup> The theory assumes the validity of the three-step model for photoemission (i.e., the ability to separate the bulk photoionization process from the transport of the photoelectrons to the surface and their escape into the vacuum) and also assumes a direct-transition picture.<sup>53</sup> In a direct transition, it is assumed that the momentum of an electron excited from one band to another is unchanged (since the photon momentum is negligible in comparison). Thus

$$E_f = E_i + h\nu, \quad (1)$$

$$k_f = k_i, \quad (2)$$

where  $E_f$  and  $E_i$  are the final- and initial-state energies of the electron in the solid,  $h\nu$  is the photon energy, and  $k_f$  and  $k_i$  are the final- and initial-state wave vectors, respectively. The goal of an ARUPS experiment is to map  $E_i(k_i)$  by measuring  $E(k)$  in vacuum (i.e., the kinetic energy and direction of the photoelectron in vacuum). To relate these we either need to know or to assume the dispersion of the final state inside the crystal,  $E_f(k_f)$ . If suitable calculated final-state bands are not available, as is the case for most materials, one generally assumes a free-electron final state inside the crystal:

$$E_f(k_f) = \hbar^2 k_f^2 / 2m - V_0 \quad (V_0 > 0), \quad (3)$$

where  $m$  is the mass of the electron and  $V_0$  is a constant positive inner potential referenced to the vacuum level which defines the zero of the free-electron final-state band. The free-electron final state has been shown to be a reasonable approximation in the case of metals<sup>31–38</sup> and some semiconductors.<sup>40</sup>

The final state in the crystal must then be related to the experimentally observed energy and direction of the photoelectron. This is done by using the fact that upon exiting the solid the component of  $k_f$  parallel to the surface,  $k_{f\parallel}$ , is conserved to within a surface reciprocal-lattice vector.<sup>54</sup> With this knowledge, simple kinematic equations for the behavior of the electron can be derived;<sup>29,40</sup> these become even simpler if only electrons emitted normal to the surface are detected. For this case of normal emission, we have

$$\begin{aligned} k_{f\parallel} &= 0, \\ k_i^{\perp} &= k_f^{\perp} = 0.51(E + V_0)^{1/2} \text{ \AA}^{-1}, \end{aligned} \quad (4)$$

where the free-electron mass is assumed and  $E$  and  $V_0$  are expressed in eV. [As written, Eq. (4) ignores any umklapp processes; these can be included trivially if necessary.<sup>29,40</sup>] Thus by measuring the way in which the kinetic energy of a particular feature in an energy-

distribution curve varies as the photon energy is varied, we obtain different values of  $k_i^{\perp}$  ( $=k_i$  if  $k_{f\parallel}=0$ ), and can thus map out the dispersion along a direction in  $k$  space normal to the surface.<sup>30,38</sup> (Other directions in  $k$  space can be probed by examining the off-normal emission. If this emission is monitored in a mirror plane of the surface, simple symmetry selection rules assist in the interpretation of the spectra.<sup>55</sup>)

The analysis outlined above can be complicated by the presence of umklapp peaks (both surface and bulk), Auger peaks, satellite peaks, surface-state emission, resonant photoemission, and density-of-states effects.<sup>41</sup> Fortunately, most of these effects are easily distinguished from the direct-transition peaks by virtue of their non-dispersive nature.

## 3. Normal emission from $(10\bar{1}2)$ surfaces of $\text{Ti}_2\text{O}_3$ and $\text{V}_2\text{O}_3$ : Theoretical considerations

As will be discussed in Sec. IV, the only low-defect-density cleavage surface for both  $\text{Ti}_2\text{O}_3$  and  $\text{V}_2\text{O}_3$  single crystals is the  $(10\bar{1}2)$  plane (hexagonal notation). [In trigonal notation, the  $(10\bar{1}2)$  plane indexes as  $(411)$ .<sup>56</sup>] All ARUPS spectra presented here are for emission normal to this surface. As detailed earlier, both crystals have a trigonal Bravais lattice with the  $D_{3d}^6(R3C)$  space group.<sup>1,2</sup> The unit-cell dimensions for  $\text{V}_2\text{O}_3$  are  $a_H = 4.95 \text{ \AA}$ ,  $c = 14.00 \text{ \AA}$ ,<sup>57</sup> and for  $\text{Ti}_2\text{O}_3$  they are  $a_H = 5.16 \text{ \AA}$ ,  $c = 13.61 \text{ \AA}$ .<sup>24</sup> The three-dimensional Brillouin zone, after Slater,<sup>58</sup> is shown in Fig. 2. Using the trigonal basis vectors defined by Slater,<sup>58</sup> it can be shown that the direction normal to the  $(10\bar{1}2)$  plane lies in the  $xz$  plane and intersects a  $\Gamma$  point  $5.15 \text{ \AA}^{-1}$  from the  $\Gamma_0$  origin for  $\text{V}_2\text{O}_3$  and  $5.04 \text{ \AA}^{-1}$  for  $\text{Ti}_2\text{O}_3$ ; this  $\Gamma$  point is five zones from the origin. Thus the direction in  $k$  space probed by the normal-emission experiment from the  $(10\bar{1}2)$  surface is the  $\Gamma_0 B \Gamma_5$  line, as shown in Fig. 3. Unfortunately, none of the available band-structure calculations give dispersions along this direction.<sup>2,10</sup> However, as shown in Fig. 3, the calculated directions (the  $x$  and  $z$  axes) do intersect the experimentally probed line, so that

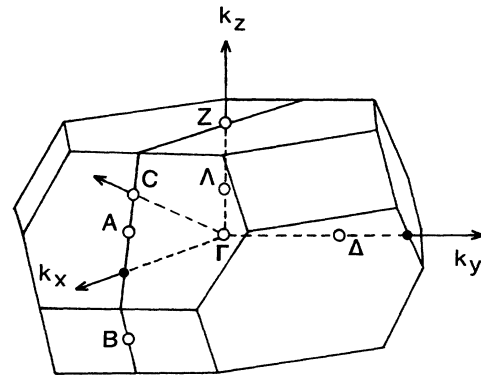


FIG. 2. Bulk Brillouin zone for a rhombohedral Bravais lattice (after Ref. 58). The direction perpendicular to the  $(10\bar{1}2)$  plane is the line marked  $\Gamma C$ .

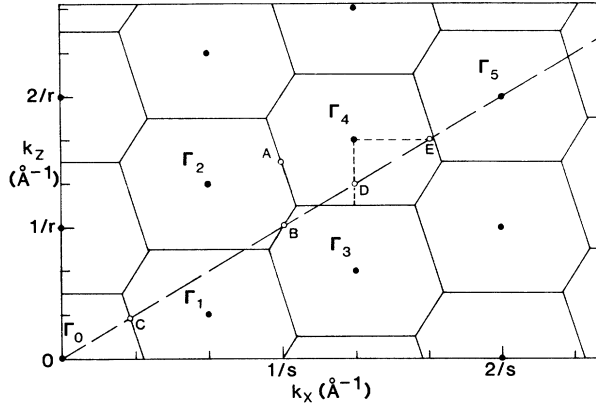


FIG. 3.  $xz$  cut through the bulk Brillouin zone of Fig. 2. The direction perpendicular to the  $(10\bar{1}2)$  plane is the dashed line from  $\Gamma_0$  through  $\Gamma_5$ . The scale is appropriate for  $\text{Ti}_2\text{O}_3$ .  $s$  and  $r$  are the fundamental units of the rhombohedral basis vectors (Ref. 58): for  $\text{V}_2\text{O}_3$ ,  $s = 2.86 \text{ \AA}$  and  $r = 4.67 \text{ \AA}$ , and for  $\text{Ti}_2\text{O}_3$ ,  $s = 2.98 \text{ \AA}$  and  $r = 4.54 \text{ \AA}$ . Thus in  $k$  space  $|\Gamma_0\Gamma_5| = 5.15 \text{ \AA}^{-1}$  in  $\text{V}_2\text{O}_3$  and  $5.05 \text{ \AA}^{-1}$  in  $\text{Ti}_2\text{O}_3$ .

comparisons between experiment and theory be can be made at selected points; this is done in Sec. VI. [Off-normal spectra were not taken here. Since the  $(10\bar{1}2)$  surface does not contain a mirror plane, we decided to limit our first attempt at a band mapping of these materials to a normal-emission experiment.]

### B. Resonant photoemission

Resonant photoemission is the phenomenon whereby photoemission from  $d$ -electron states is enhanced when the energy of the incident photons exceeds a threshold value related to the interband transition energy between a low-lying core level (in this study, a cation  $3p$  level) and empty valence-band states near the Fermi level. This effect has been the subject of intensive investigation recently, and a comprehensive review has been published by Davis.<sup>59</sup> Much of the work in this field has concentrated on the heavy ( $Z > 25$ ) transition metals and their compounds and on the rare-earth metals. In contrast, there are only a handful of studies concerned with resonance in the light ( $Z < 25$ ) transition-metal compounds.<sup>13,49,60-62</sup> We report here the observation of  $3p \rightarrow 3d$  resonance effects in  $3d$  photoemission from both  $\text{Ti}_2\text{O}_3$  and  $\text{V}_2\text{O}_3$  single crystals.

Resonant photoemission occurs when a separate ionization mechanism exists which leaves the system in the same final state as does conventional photoemission. For emission from a  $d$  state, the latter process can be written in an atomic picture as

$$3p^6 3d^n + h\nu \rightarrow 3p^6 3d^{n-1} + e^-(\epsilon),$$

where a photon of energy  $h\nu$  ionizes the neutral atom and ejects a  $3d$  electron with kinetic energy  $\epsilon$ . If the photon energy is equal to, or slightly greater than, the  $3p$ - $3d$  interband separation, we can get optical absorption,

$$3p^6 3d^n + h\nu \rightarrow [3p^5 3d^{n+1}]^*,$$

where the asterisk indicates an atom or ion in an excited state. This state can decay a number of mechanisms; the one which is responsible for the resonance is direct recombination,

$$[3p^5 3d^{n+1}]^* \rightarrow 3p^6 3d^{n-1} + e^-(\epsilon),$$

where the excited state transfers all of its energy to the emitted electron in an Auger-type decay. The final state following a direct recombination is the same as that following conventional  $3d$  photoemission, and it is interference between these two phenomena that is the origin of resonant photoemission.

In the light transition metals, the onset resonance in  $3d$  photoemission is delayed, occurring at photon energies higher than the  $3p$ - $3d$  interband separation.<sup>60-64</sup> This delay is postulated to be due to the exchange interaction which increases the energy of the  $[3p^5 3d^{n-1}]^*$  excited state.<sup>60-65</sup> The delay may be as much as to 10-15 eV and has been observed in Ti,<sup>60,63</sup> TiN,<sup>61,62</sup> and V,<sup>63</sup> among others.

The  $d$  electron emitted following deexcitation of the  $[3p^5 3d^{n+1}]^*$  state by direct recombination has the same initial state as does the  $d$  electron emitted by conventional photoemission. This is an important point since it implies that the resonant photoemission feature should show the dispersion of the  $d$  band if such dispersion exists. The intensity of the  $d$  emission may thus change dramatically during resonance, but the binding energy will just be that of the bulk  $d$  band. This has been observed previously in the ARUPS spectra of  $\text{UPd}_3$ .<sup>66</sup> However, some authors claim that resonant photoemission features should be dispersionless.<sup>45</sup> Nondispersive resonances have indeed been seen in the ARUPS spectra from a variety of materials,<sup>45,62,67</sup> but this is most likely a density-of-states effect, occurring at higher photon energies where  $k$  broadening of the spectra becomes important. We will not discuss the details of the resonance as displayed by these materials in this paper; a forthcoming publication will be devoted to the resonant photoemission process alone.<sup>21</sup>

## IV. EXPERIMENTAL METHODS

### A. Sample preparation

The single-crystal  $\text{V}_2\text{O}_3$  in this experiment was grown by Dr. D. Buttrey of Purdue University, and the  $\text{Ti}_2\text{O}_3$  by T.B. Reed of Lincoln Laboratory. Both materials cleave along only one direction, exposing the  $(10\bar{1}2)$  face.<sup>11,12</sup> In the case of  $\text{Ti}_2\text{O}_3$  ( $10\bar{1}2$ ) it is possible to reproduce a cleaved surface by a laborious sputter-anneal technique;<sup>68,69</sup> no analogous process has been found for  $\text{V}_2\text{O}_3$  ( $10\bar{1}2$ ).<sup>70</sup> Since enough material was available to cleave, this was the method chosen to obtain stoichiometric surfaces approaching as closely as possible a truncation of the bulk lattice. In general,  $\text{Ti}_2\text{O}_3$  cleaves much better than  $\text{V}_2\text{O}_3$ . Both surfaces display  $(1 \times 1)$  low-energy electron-diffraction (LEED) patterns, but those from  $\text{Ti}_2\text{O}_3$  are generally of higher quality. The crystals were oriented using Laue x-ray diffraction and cut into rods approximately  $3 \times 3 \times 10 \text{ mm}^3$  with the long axis perpen-

dicular to the  $(10\bar{1}2)$  direction. Cleavage grooves were cut every 1.0 mm on the side of the rods to facilitate cleavage. All crystals were cleaved in the experimental chamber at pressures  $< 1.5 \times 10^{-10}$  torr.

### B. Apparatus

All the experiments reported here were performed on beamline U14 at the National Synchrotron Light Source (NSLS), Brookhaven National Laboratory. Photons of energy  $30 < h\nu < 100$  eV from a plane grating monochromator were used in this study. Angle-integrated spectra were taken using a cylindrical mirror analyzer (CMA) and angle-resolved spectra with a Vacuum Generators (VG) model 424 hemispherical electron spectrometer. Typical resolutions for both spectrometers were of the order of 200 meV at  $h\nu = 30$  eV and 600 meV at  $h\nu = 100$  eV. Most angle-resolved spectra were taken with the photon beam incident at  $45^\circ$  to the sample normal; this gives mixed *s*- and *p*-polarized light. The closest to normal incidence (*s* polarization) that the experimental arrangement allowed was  $\approx 35^\circ$  ( $0^\circ$  is normal). Angle-integrated spectra were taken with the photon beam incident at approximately  $60^\circ$  off the sample normal and the CMA axis at  $45^\circ$ . Base pressures during measurements were less than  $1.5 \times 10^{-10}$  torr. All spectra presented here are referenced to the Fermi level ( $E_F$ ), which was determined both by the emission from an automatically clean gold film and from the angle-integrated  $\text{V}_2\text{O}_3$  spectra themselves. In addition, unless otherwise noted, all spectra presented are normalized to constant O  $2p$  emission (i.e., the area under the O  $2p$  peaks, after subtraction of a linear background). Pass energies were fixed at 25 eV for the CMA and 15 eV for the VG detector.

## V. RESULTS

### A. Angle-resolved photoemission from $\text{Ti}_2\text{O}_3$

Angle-resolved photoemission spectra for cleaved  $\text{Ti}_2\text{O}_3(10\bar{1}2)$  are shown in Figs. 4 and 5. Figure 4 shows a series of normal-emission spectra taken with photon energies between 39 and 90 eV and with the photon beam incident at  $35^\circ$  to the sample normal. Figure 5 compares spectra from obtained at the same photon energy and emission angle ( $0^\circ$ ) but different incident-photon angles. The general features of all the spectra are similar. Emission from the Ti  $3d a_{1g}$  band lies just below  $E_F$ . Emission from the O  $2p$  band occurs because 4 and 10 eV below  $E_F$ . These bands are separated by a region of broad, low-intensity emission. As the photon energy is increased, changes occur in the emission from each of these regions. Resonant photoemission is dramatically displayed by the Ti  $3d$  feature just below  $E_F$ . For  $h\nu > 42$  eV, there is a huge enhancement of this emission (Fig. 4). As the photon energy is increased above the resonance maximum ( $\approx 45$  eV), the emission decreases slowly in intensity. The O  $2p$  emission also shows the effect of resonance, displaying intensity changes as the photon energy is swept. The region of the spectra between the main Ti  $3d$  emission and the broad O  $2p$  emission shows apprecia-

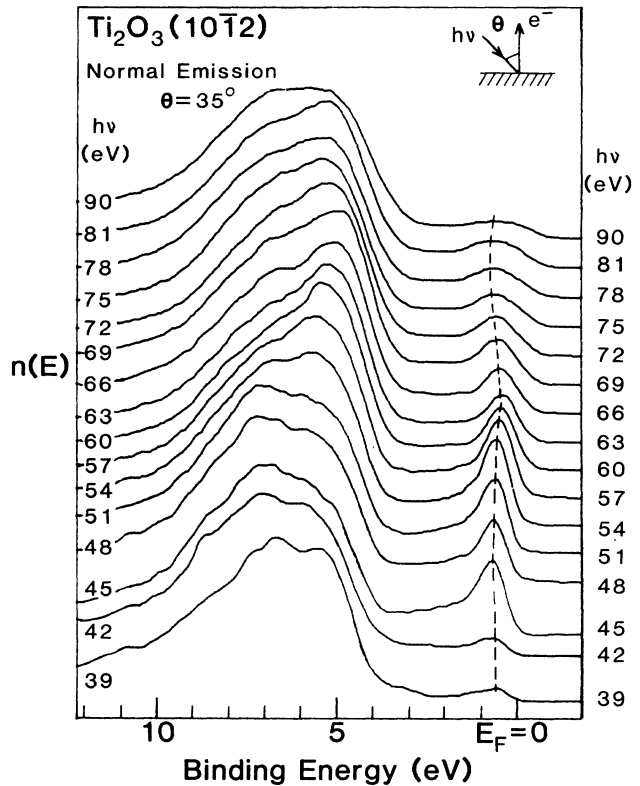


FIG. 4. Normal-emission ARUPS spectra from cleaved  $\text{Ti}_2\text{O}_3(10\bar{1}2)$  for photon energies from 39 to 90 eV.

ble variation in intensity and structure as the photon energy goes above resonance. In the available band models,<sup>1,2,10</sup> this region is an absolute bulk band gap. The O  $2p$  emission displays a broad structure at all energies, with some variations in shape with changing photon energy. These data will be discussed in Sec. VI.

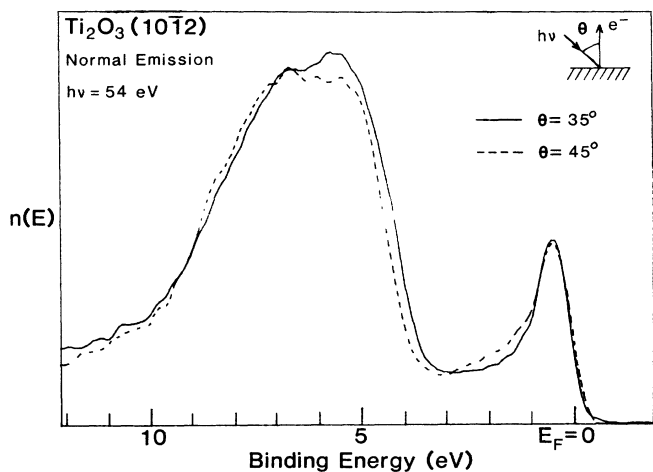


FIG. 5. Normal-emission ARUPS spectra from  $\text{Ti}_2\text{O}_3(10\bar{1}2)$  taken with  $h\nu = 54$  eV for photon angles of incidence of  $35^\circ$  and  $45^\circ$ .

### B. Angle-resolved photoemission from $V_2O_3$

Angle-resolved photoemission spectra for cleaved  $V_2O_3(10\bar{1}2)$  are shown in Figs. 6 and 7. Figure 6 shows a series of spectra taken with photon energies between 35 and 80 eV with the photon beam incident at  $45^\circ$  to the sample normal. Figure 7 shows the effect on a normal-emission spectrum taken at  $h\nu=60$  eV of varying the angle of incidence of the photons from  $35^\circ$  to  $65^\circ$ . All spectra display the same general features; a broad structureless peak at  $E_F$  due to emission from the V  $3d$  bands, and a wider and more structured peak beginning approximately 3.5–4 eV below  $E_f$  due to emission from the O  $2p$  bands. The absence of a formal band gap between these features will be discussed in Sec. VI. The spectra are seen to pass through a resonance beginning at  $h\nu \approx 46$  eV. The V  $3d$  bands show a dispersion slightly smaller than that seen for the Ti  $3d$  bands in  $Ti_2O_3$ . As for  $Ti_2O_3$ , the O  $2p$  bands show some intensity changes as the photon energy is varied.

### C. Angle-integrated spectra from $V_2O_3$

Figure 8 shows a series of angle-integrated photoemission spectra for photon energies from 40 to 65 eV. The main features are very similar to those visible in the ARUPS spectra of Fig. 6. In addition to the resonant behavior described in the preceding section, a new feature at approximately 11 eV below  $E_f$ , labeled *A*, is visible in

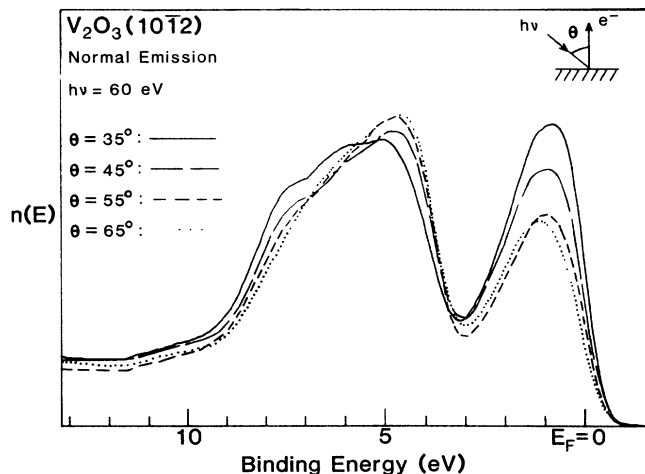


FIG. 7. Normal-emission ARUPS spectra from  $V_2O_3(10\bar{1}2)$  taken with  $h\nu=60$  eV for photon angles of incidence of  $35^\circ$  and  $65^\circ$ .

all the spectra. At higher photon energies, a second small feature labeled *B*, is visible about 2–3 eV below *A*. These data will be discussed in the next section.

## VI. DISCUSSION

The data presented in the preceding section contain information on a number of phenomena of interest in  $Ti_2O_3$

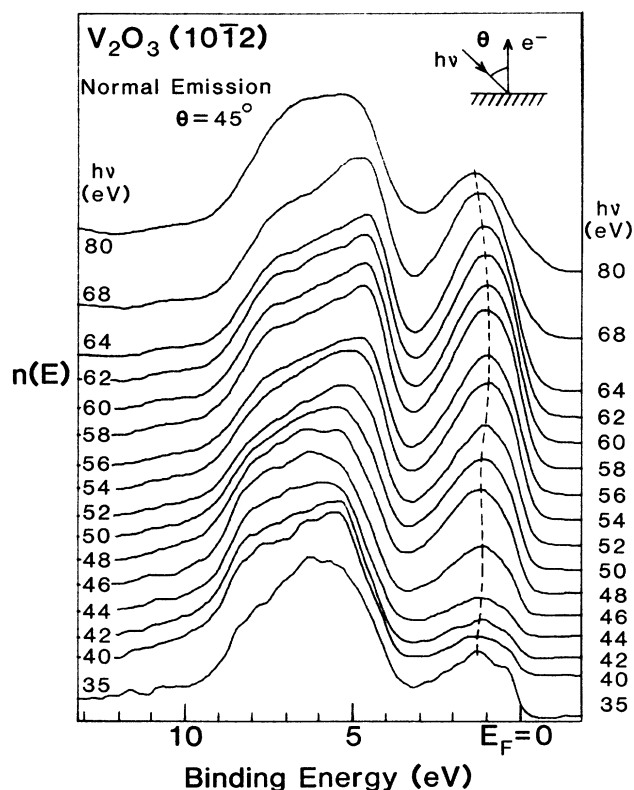


FIG. 6. Normal-emission ARUPS spectra from  $V_2O_3(10\bar{1}2)$  for photon energies from 35 to 80 eV.

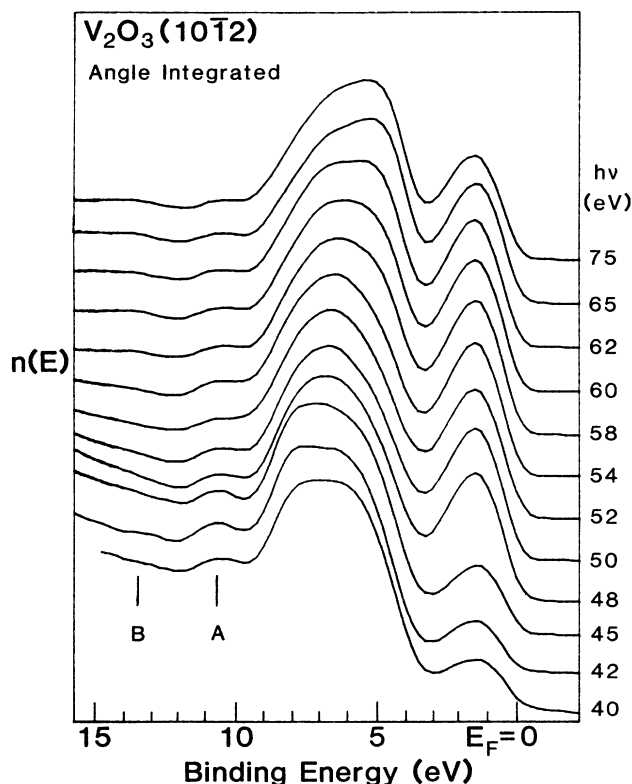


FIG. 8. Angle-integrated photoemission spectra from  $V_2O_3(10\bar{1}2)$  for photon energies between 40 and 75 eV.

and  $\text{V}_2\text{O}_3$ : the bulk electronic density of states, the nature of the band gap between the cation  $d$  levels and the oxygen  $p$  levels, the polarization dependence of the photoemission spectra, the bulk band dispersion, and the resonant photoemission phenomenon. We will discuss all but the last of these topics in the present paper; resonant photoemission is considered in a separate publication.<sup>21</sup>

### A. Bulk band dispersion in $\text{Ti}_2\text{O}_3$ and $\text{V}_2\text{O}_3$

In general, the angle-resolved spectra from both  $\text{Ti}_2\text{O}_3$  and  $\text{V}_2\text{O}_3$  obtained in this study are similar to those obtained in an angle-integrated mode. The photoemission spectra from these materials have been shown previously to be primarily representative of the bulk electronic structure as opposed to any specifically surface-related structure.<sup>12</sup> The similarity between the angle-integrated and angle-resolved spectra indicates that even at low photon energies density-of-states effects are important in these materials. However, as illustrated in Figs. 4 and 6, there is a small but significant dispersion of the  $3d$  bands in  $\text{Ti}_2\text{O}_3$  and  $\text{V}_2\text{O}_3$  as the photon energy is varied; this cannot be explained as a density-of-states effect. Additionally, changes in the O  $2p$  emission feature with photon energy can be seen in both materials, but the emission is too broad to extract unambiguous O  $2p$  band dispersions.

Our goal is to determine the dispersion of the initial-state cation  $d$  bands and relate it to the available band-structure calculations.<sup>2,10</sup> As was discussed in Sec. III A, this requires either calculated final-state band dispersions or an analytic functional form for the final state in order to extract a  $k$  vector from the observed electron direction and kinetic energy. Since we do not have calculations for the final-state dispersions further than 8 eV above  $E_f$ , we must assume a free-electron final state and proceed as detailed in Sec. III A. Ashkenazi and Chuchem<sup>2</sup> (AC) use a value of 21.76 eV for the inner potential,  $V_0$ , in both  $\text{Ti}_2\text{O}_3$  and  $\text{V}_2\text{O}_3$  in their linear combination of atomic orbitals (LCAO) calculation of the band structure of these materials; we thus used that value for  $V_0$  in Eq. (4). As discussed earlier, the direction in  $k$  space probed in our normal-emission experiments is  $\Gamma_0 B \Gamma_5$  (see Fig. 3), and from Eq. (4) it can be shown that the dispersion along this direction can be examined between roughly the points  $D$  and  $\Gamma_5$ . From each spectrum presented in Fig. 4 for  $\text{Ti}_2\text{O}_3$  and Fig. 6 for  $\text{V}_2\text{O}_3$ , we can extract a binding energy for the cation  $d$  emission relative to  $E_f$  and a corresponding kinetic energy relative to the vacuum level. Using the latter in Eq. (4) gives the  $k$  vector associated with a given electron. In this manner we generate  $d$ -band dispersion curves (plots of cation  $d$ -state binding energy versus  $k$  vector) for  $\text{Ti}_2\text{O}_3$  and  $\text{V}_2\text{O}_3$ , shown in Figs. 9 and 10, respectively. (Also indicated in Fig. 9 is the dispersion curve generated from a set of normal-emission ARUPS spectra from  $\text{Ti}_2\text{O}_3$  where the angle of incidence of the photons was equal to  $45^\circ$ ; the original spectra are not shown.)

As noted earlier, neither of the available band-structure calculations provide dispersions along the

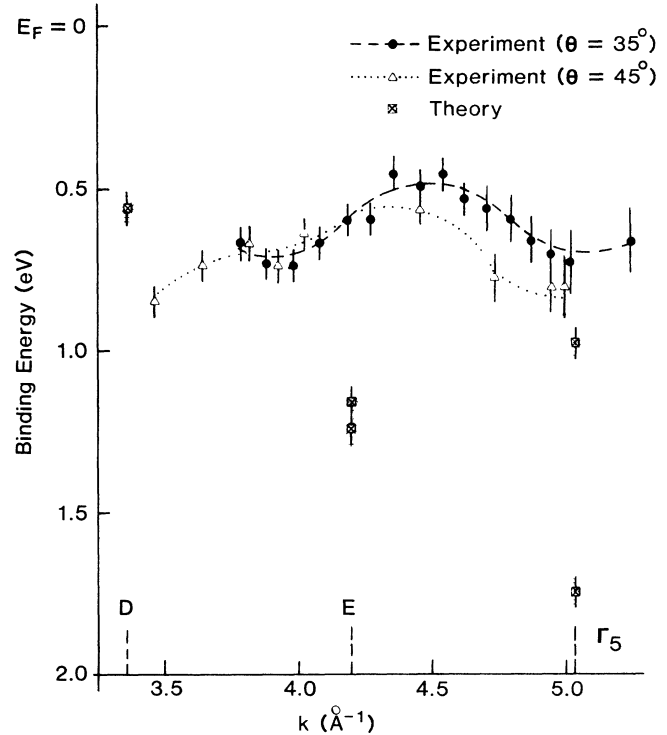


FIG. 9. Cation  $d$ -band dispersion in  $\text{Ti}_2\text{O}_3$ . Measured dispersions are indicated by  $\bullet$  and  $\triangle$ ; the lines shown are merely guides to the eye. Theoretically predicted points from Ref. 10 are also shown. See text for details.

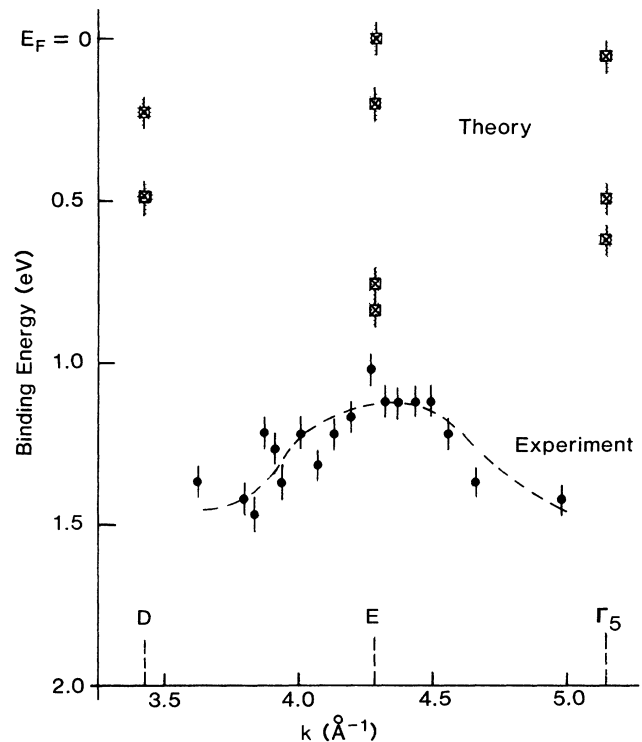


FIG. 10. Cation  $d$ -band dispersion in  $\text{V}_2\text{O}_3$ . Measured dispersions is indicated by  $\bullet$ . Theoretically predicted points from Ref. 10 are also shown. See text for details.

direction that we are probing in  $k$  space. However, there are three points at which the calculations intersect the experimentally probed direction; these are at  $D$ ,  $E$ , and  $\Gamma_5$ , where  $D$  and  $E$  are the intersections of the  $\Gamma_0 B \Gamma_5$  ( $10\bar{1}2$ ) direction with the  $k_z$  and  $k_x$  axes in the fourth zone, respectively, and  $\Gamma_5$  the center of zone 5. Since the calculations of Ashkenazi and Weger<sup>10</sup> (AW) include the effects of electron correlation, we compare our experimentally determined dispersions to those calculations. The predicted binding energies of the  $d$  band at points  $D$ ,  $E$ , and  $\Gamma_5$ , as extracted from the published curves of AW, are marked on Figs. 9 and 10 for  $\text{Ti}_2\text{O}_3$  and  $\text{V}_2\text{O}_3$ , respectively. Where more than one band exists at a particular  $k$ -vector value in the calculations, all of the binding energies are marked.

There is little absolute agreement between the observed and calculated binding energies of the cation  $d$  electrons for either material. As discussed in AC and AW, the influence of the ligand levels is treated only roughly, thus allowing some flexibility in "adjusting" the calculations to fit experimental data.<sup>28</sup> Indeed, AC are required to increase the binding energy of the calculated conduction band in  $\text{V}_2\text{O}_3$  by almost 1 eV in order to get reasonable agreement between the calculations and the optical data of Shuker and Yacoby.<sup>28</sup> A shift of this magnitude is also required to bring the calculations of AW into closer agreement with our measurements for  $\text{V}_2\text{O}_3$  (Fig. 10). In  $\text{Ti}_2\text{O}_3$ , the agreement between theory and experiment (Fig. 9) becomes progressively worse as the  $k$  vector increases. However, our experimental resolution decreases significantly as the photon energy increases (see Fig. 4), making the assignment of a unique binding energy to the Ti  $3d$  emission at higher energies more difficult.

More significant than the numerical agreement of the calculated and measured binding energies is the observation of any dispersion at all. In both  $\text{Ti}_2\text{O}_3$  and  $\text{V}_2\text{O}_3$  the dispersions are small ( $< 0.4$  eV), but nonetheless support a band model for the electronic structure of these materials. Additionally, as discussed in Sec. IV,  $\text{Ti}_2\text{O}_3$  is an ideal material on which to test the applicability of ARUPS to investigations of the band structure of metal oxides. It is clear from this study that ARUPS can be used profitably on this class of materials, providing direct information on the bulk band dispersion.

### B. Polarization effects in $\text{Ti}_2\text{O}_3$ and $\text{V}_2\text{O}_3$

The effect of changing the angle of incidence of the photons on the normal-emission spectra of  $\text{Ti}_2\text{O}_3$  can be seen in Fig. 5, where the spectra taken with photons incident at  $45^\circ$  and  $35^\circ$  for  $h\nu=54$  eV are shown superimposed. The spectra are normalized to the same O  $2p$  emission intensity. It is clear that varying the angle by this amount results in only slight changes in the spectra. The location of the Ti  $3d$  maximum is unchanged, although its full width at half maximum (FWHM) has increased somewhat. Emission from the nonbonding states at the top of the O  $2p$  band decreases in intensity, with a consequent narrowing of the band, as the  $p$  component of the photon polarization increases; this sensitivity of the O  $2p$  states to polarization is not displayed by the Ti  $3d$  or-

bitals. It is noteworthy that  $\text{Ti}_2\text{O}_3$  displays none of the large sensitivity to polarization that has been found in TiN.<sup>43</sup>

Figure 7 shows the normal-emission spectra from  $\text{V}_2\text{O}_3$  taken with 60-eV photons incident at angles between  $35^\circ$  and  $65^\circ$  to the surface normal. Much more dramatic changes occur here with changes in photon polarization than occurred in  $\text{Ti}_2\text{O}_3$ . The V  $3d$  emission is enhanced with respect to the O  $2p$  emission as the angle of incidence approaches  $0^\circ$  (normal incidence). In addition, the V  $3d$  peak shifts to higher binding energy as the photons approach grazing incidence. The structure of the O  $2p$  band also changes, with emission from the nonbonding O  $2p$  orbitals at the top of the band being favored at high angles of incidence (grazing incidence). This is the opposite of the effect observed in  $\text{Ti}_2\text{O}_3$ . The spectra become increasingly surface sensitive as grazing incidence is approached, which adds to the complexity of the changing polarization selection rules. At present we are unable to account for these observations.

### C. Bulk-band-gap emission in $\text{Ti}_2\text{O}_3$ and $\text{V}_2\text{O}_3$

The empirical band structure for  $\text{Ti}_2\text{O}_3$  illustrated in Fig. 1 indicates that there is a separation of approximately 2.5 eV between the bottom of the Ti  $3d a_{1g}$  band and the top of the O  $2p$  band,<sup>1</sup> based on optical data.<sup>1,23</sup> However, angle-integrated ultraviolet-photoemission (UP) spectra of cleaved single-crystal  $\text{Ti}_2\text{O}_3$  display significant emission above the background in this region.<sup>12,13,69,71</sup> When the photon energy is swept through the  $3p \rightarrow 3d$  resonance, this band-gap emission is also seen to resonate, indicating a significant cation component.<sup>13</sup> As can be seen in Fig. 4, identical behavior is observed in the ARUPS spectra. In previous studies<sup>12,13</sup> it was speculated that either this emission originates from a surface state (with considerable  $d$ -band character, as evidenced by the resonant behavior of the emission) or that the bulk band gap is much narrower than optical measurements indicate. Unfortunately, the ARUPS spectra do not clarify this issue; no resolvable surface-state peak was observed at any photon energy in normal emission. The optically deduced band gap of 2.5 eV is too large for hole lifetime broadening of the valence-band emission spectra to account for the band-gap emission. This mechanism has been postulated as the reason that no band gap is observed between the Ir  $5d$  and O  $2p$  emission in the valence-band x-ray-photoemission (XP) spectra of the rutile  $5d$  transition-metal oxide  $\text{IrO}_2$ .<sup>72</sup> Considering that for  $\text{IrO}_2$  band gap is almost 1 eV narrower than that in  $\text{Ti}_2\text{O}_3$  and that our resolution at low photon energies is approximately twice as good as that of the XPS study,<sup>72</sup> we conclude that in  $\text{Ti}_2\text{O}_3$  lifetime broadening is not sufficient to explain the bulk-band-gap emission; the origin of this emission remains undetermined.

We cannot make as definitive a statement in the case of  $\text{V}_2\text{O}_3$ . As can be seen in Fig. 6, there is, as in  $\text{Ti}_2\text{O}_3$ , no formal band gap between the V  $3d$  and O  $2p$  emission, although again theory predicts that one should exist.<sup>1</sup> However, in this case the width of the  $d$ -band emission is large enough to make a hole lifetime broadening mecha-

nism more plausible; indeed the spectra look quite similar to those of  $\text{IrO}_2$ . Finally, studies of the effect of deliberately creating defects on the surfaces of these materials indicate that the anomalous band-gap emission is not primarily defect related.<sup>11</sup>

#### D. Valence-band satellites in $\text{V}_2\text{O}_3$

Most transition-metal compounds exhibit satellite emission associated with both cation core and valence levels.<sup>59</sup> For the light- ( $Z < 25$ ) transition-metal compounds, two competing theories exist for the origin of these satellites.<sup>73–75</sup> The first, by de Boer, Haas, and Sawatzky,<sup>73</sup> is an exciton model in which the polarization of the ligands is responsible for screening the cation hole; the satellite is then due to an electron-hole pair (exciton) on the ligand. The mechanism for satellite formation in transition-metal compounds in this model is the following. The metal atom loses a core electron via photoemission, leaving behind a core hole which acts as a  $Z + 1$  impurity with respect to the valence electrons.<sup>73</sup> There are two expected final states for this system. One consists of the ligand states polarized towards the cation but with no change in the population of the ligand states. The second consists of both a polarization of the ligand states and population of a higher, previously empty ligand level. Consequently, this second state corresponds to an electron-hole pair on the ligand. The existence of these two final states leads to two peaks in the photoemission spectra of metal core levels. In contrast with this mechanism is that of charge-transfer screening. Veal and Paulikas<sup>74</sup> have constructed a theory for satellites in insulating transition-metal oxides which involves ligand-to-metal charge transfer, with the main photoemission line corresponding to emission from a fully relaxed (locally screened) state, and the satellite emission arising from less fully screened states. However, the model of cation-to-ligand charge transfer which is adequate for heavy- ( $Z > 25$ ) transition-metal oxides is inadequate for the high-energy ( $\geq 10$  eV) satellites in light oxides<sup>73</sup> and we shall not discuss it further here.

We do not observe any valence-band satellites in the spectrum from  $\text{Ti}_2\text{O}_3$  (see Fig. 4 and Ref. 13), but a satellite has been reported 13 eV below the main-line emission in XPS spectra of the Ti  $2p$  core level.<sup>13</sup> A possible reason for the lack of a valence-band satellite in  $\text{Ti}_2\text{O}_3$  is the presence of only one  $d$  electron per cation, which would imply a low intensity for this feature.<sup>13</sup> Since  $\text{V}_2\text{O}_3$  has a  $3d^2$  configuration, we might expect to be able to observe a valence-band satellite in this material where one could not be seen in  $\text{Ti}_2\text{O}_3$ . A feature, which we have labeled *A*, is clearly visible in the angle-integrated spectra of Fig. 8 at higher binding energy than the O  $2p$  band. This feature lies 10.8 eV below  $E_F$ , or 9.3 eV below the V  $3d$  emission. This feature is not resolved in the ARUPS data of Fig. 6; what is observed is a broad asymmetrical tail on the high-binding-energy side of the O  $2p$  emission. Because of this asymmetry, the width of the O  $2p$  emission (as measured above a smooth background) is considerably larger in the ARUPS spectra than in the angle-integrated spectra. However, the width of the O  $2p$  emis-

sion in the ARUPS spectra (including the asymmetric tail, Fig. 6) is identical to the sum of the width of the O  $2p$  emission and feature *A* in the angle-integrated spectra (Fig. 8). So while not resolved, we believe that feature *A* is also present in the angle-resolved data.

This feature has not been identified in previous angle-integrated UPS spectra of cleaved  $\text{V}_2\text{O}_3$ .<sup>11</sup> However, the emission from the O  $2p$  band in that work exhibits the characteristic asymmetrical tail, and the width of the band is just that of our angle-integrated spectra if we include feature *A*. Thus we believe that the same feature is present in the data of Ref. 11, although it was not resolved, leading to an overestimation of the O  $2p$  bandwidth. Honig *et al.*<sup>19</sup> use a Gaussian at approximately 11 eV as part of the deconvolution of their valence-band XPS data, although they do not give a physical origin for this emission. Werfel and Brummer<sup>14</sup> observe a feature in their valence-band XPS spectra of sputtered single-crystal  $\text{V}_2\text{O}_3$  at 10.7 eV; they assign it to a plasmon loss. It is not known whether a similar feature exists in the data of Vasudevan *et al.*<sup>20</sup> as they do not publish data for the appropriate energy region. In any case their surfaces are heavily oxidized, as can be seen from the relative V  $3d$ -to-O  $2p$  intensity ratio. Beatham *et al.*<sup>18</sup> do not observe any emission in the region 10–12 eV below  $E_f$  in their He I spectra of polycrystalline  $\text{V}_2\text{O}_3$ ; they do observe a feature in their valence-band XPS spectra approximately 13.5 eV below  $E_F$ , but do not identify it. Sawatzky and Post<sup>17</sup> do not publish data in the appropriate energy range. In electron-energy-loss-spectroscopy (EELS) measurements, a feature at 10 eV is seen in the spectra from both  $\text{V}_2\text{O}_3$  powders<sup>76</sup> and single crystals.<sup>77</sup> In the former case it was tentatively assigned to a surface-plasmon loss, while in the latter it is identified as a bulk transition from the O  $2p$  band to empty V  $3d$  states.

Based on this observation of a bulk transition in the EELS spectra at 10 eV from single-crystal  $\text{V}_2\text{O}_3$ ,<sup>77</sup> we tentatively assign the feature marked *A* in Fig. 8 to an exciton satellite of the main V  $3d$  emission, according to the model of de Boer *et al.*<sup>73</sup> This model requires that exciton satellites occur at the same energy as peaks in EELS spectra or optical-absorption spectra. A second weak feature, labeled *B*, is visible in the higher-photon-energy spectra of Fig. 8, approximately 14 eV below  $E_F$ . No corresponding feature is identified in the EELS spectra of Ref. 77, but the 10-eV loss is very broad and could easily include a contribution at this energy. Thus the existence of a bulk loss at the energy equivalent to peak *B* is undetermined and the feature remains unidentified.

## VII. CONCLUSIONS AND SUMMARY

We have studied the bulk band structure of the corundum transition-metal oxides  $\text{Ti}_2\text{O}_3$  and  $\text{V}_2\text{O}_3$  using both angle-integrated and angle-resolved photoemission and synchrotron radiation. The density of states for these materials determined in this study is similar to that obtained previously using He I and He II radiation. Emission from the cation  $d$  bands, 1.5 eV wide in  $\text{Ti}_2\text{O}_3$  and 3 eV wide in  $\text{V}_2\text{O}_3$ , occurs close to  $E_F$ . Emission from the

O  $2p$  band begins about 3.5 eV below  $E_F$ . For  $V_2O_3$  we have shown that the width of the O  $2p$  band is about 2.5 eV narrower than was previously thought. This is due to the resolution of a separate emission feature at the bottom of the O  $2p$  band which is interpreted as a valence-band satellite.

Angle-resolved photoemission has been used to study bulk band dispersion in both  $Ti_2O_3$  and  $V_2O_3$ . The  $d$  bands of these materials are relatively flat, and consequently only small dispersions were observed. However, the observation of any dispersion at all supports the validity of a band model for the electronic structure of these materials. Large discrepancies were observed between the calculated  $d$ -band binding energies<sup>10</sup> and our measurements; these are thought to arise from inadequacies in the theory. In both materials the O  $2p$  band exhibited complex behavior as the photon energy was swept in a normal-emission experiment. This behavior precluded the determination of any unambiguous and credible O  $2p$  band dispersion.

Finally, resonant photoemission was observed from both of these materials as the photon energy was swept

through the respective cation  $3p \rightarrow 3d$  optical-absorption edges. A detailed analysis of the resonant photoemission data is presented elsewhere.<sup>21</sup>

#### ACKNOWLEDGMENTS

The authors are pleased to acknowledge R. J. Lad both for assistance during the course of the data acquisition and for many useful discussions. We would also like to thank R. F. Garrett, M. J. Sagurton, and G. P. Williams of NSLS for helpful and friendly advice, and E. Kneeder, also of NSLS, for invaluable and dedicated technical assistance. This work was partially supported by the U.S. National Science Foundation under Solid State Chemistry Grants Nos. DMR-82-02727 and DMR-87-11423. Research was carried out at the National Synchrotron Light Source, Brookhaven National Laboratory, which is supported by the U.S. Department of Energy, Division of Materials Sciences and Division of Chemical Sciences, under Grant No. DE-AC02-76-CH00016.

\*Present address: Department of Physics, University of Oregon, c/o National Synchrotron Light Source, Building 725-U4, Brookhaven National Laboratory, Upton, NY 11973.

<sup>1</sup>J. B. Goodenough, *Prog. Solid State Chem.* **5**, 145 (1972), and references therein.

<sup>2</sup>J. Ashkenazi and T. Chuchen, *Philos. Mag.* **32**, 763 (1975).

<sup>3</sup>P. Hertel and J. Appel, *Phys. Rev. B* **33**, 2098 (1986).

<sup>4</sup>C. Castellani, C. R. Natoli, and J. Ranninger, *Phys. Rev. B* **18**, 5001 (1978).

<sup>5</sup>C. Castellani, C. R. Natoli, and J. Ranninger, *Phys. Rev. B* **18**, 4967 (1978).

<sup>6</sup>C. Castellani, C. R. Natoli, and J. Ranninger, *J. Phys. (Paris) Colloq.* **37**, C4-199 (1976).

<sup>7</sup>J. Ashkenazi and M. Weger, *Adv. Phys.* **22**, 207 (1973).

<sup>8</sup>H. J. Zeiger, *Phys. Rev. B* **11**, 5132 (1975).

<sup>9</sup>N. F. Mott, *Metal Insulator Transitions* (Taylor and Francis, London, 1974).

<sup>10</sup>J. Ashkenazi and M. Weger, *J. Phys. (Paris) Colloq.* **37**, C4-189 (1976).

<sup>11</sup>R. L. Kurtz and V. E. Henrich, *Phys. Rev. B* **28**, 6699 (1983).

<sup>12</sup>R. L. Kurtz and V. E. Henrich, *Phys. Rev. B* **25**, 3563 (1982).

<sup>13</sup>J. M. McKay, M. H. Mohamed, and V. E. Henrich, *Phys. Rev. B* **35**, 4304 (1987).

<sup>14</sup>F. Werfel and O. Brummer, *Phys. Scr.* **28**, 92 (1983).

<sup>15</sup>F. Werfel, D. Drager, and U. Berg, *Cryst. Res. Technol.* **16**, 119 (1981).

<sup>16</sup>N. Beatnam, I. L. Fragala, A. F. Orchard, and G. Thornton, *J. Chem. Soc. Faraday Trans. II* **76**, 929 (1980).

<sup>17</sup>G. Sawatzky and D. Post, *Phys. Rev. B* **20**, 1546 (1979).

<sup>18</sup>N. Beatham, A. F. Orchard, and G. Thornton, *J. Phys. Chem. Solids* **42**, 1051 (1981).

<sup>19</sup>J. M. Honig, L. L. Van Zandt, R. D. Board, and H. E. Weaver, *Phys. Rev. B* **6**, 1323 (1972).

<sup>20</sup>S. Vasudevan, M. S. Hedge, and C. N. R. Rao, *Solid State Commun.* **27**, 131 (1978).

<sup>21</sup>K. E. Smith and V. E. Henrich, *Solid State Commun.* (to be

published); *Phys. Rev. B* (to be published).

<sup>22</sup>J. M. Honig and T. B. Reed, *Phys. Rev.* **174**, 1020 (1968); L. L. Van Zandt, J. M. Honig, and J. B. Goodenough, *J. Appl. Phys.* **39**, 594 (1968).

<sup>23</sup>S. H. Shin, F. H. Pollak, T. Halpern, and P.M. Raccach, *Solid State Commun.* **16**, 687 (1975); *J. Solid State Chem.* **12**, 407 (1975).

<sup>24</sup>C. E. Rice and W. R. Robinson, *Mater. Res. Bull.* **11**, 1355 (1976).

<sup>25</sup>S. H. Shin, R. L. Aggarwal, B. Lax, and J. M. Honig, *Phys. Rev. B* **9**, 583 (1974).

<sup>26</sup>D. B. McWhan, T. M. Rice, and J. P. Remeika, *Phys. Rev. Lett.* **22**, 887 (1969).

<sup>27</sup>D. B. McWhan, J. P. Remeika, T. M. Rice, W. F. Brinkman, J. P. Maita, and A. Menth, *Phys. Rev. Lett.* **27**, 941 (1971); D. B. McWhan, J. P. Remeika, S. D. Bader, B. B. Triplett, and N. E. Phillips, *Phys. Rev. B* **7**, 3079 (1973).

<sup>28</sup>P. Shuker and Y. Yacoby, *Phys. Rev. B* **14**, 2211 (1976).

<sup>29</sup>F. J. Himpsel, *Appl. Opt.* **19**, 3964 (1980), and references therein.

<sup>30</sup>E. W. Plummer and W. Eberhardt, *Adv. Chem. Phys.* **49**, 533 (1982), and references therein.

<sup>31</sup>E. Dietz and D. E. Eastman, *Phys. Rev. Lett.* **41**, 1674 (1978).

<sup>32</sup>F. J. Himpsel and D. E. Eastman, *Phys. Rev. B* **18**, 5236 (1978).

<sup>33</sup>F. J. Himpsel, J. A. Knapp, and D. E. Eastman, *Phys. Rev. B* **19**, 2919 (1979).

<sup>34</sup>P. Thiry, D. Chandessris, J. Lecante, C. Guillot, R. Pinchaux, and Y. Petroff, *Phys. Rev. Lett.* **43**, 82 (1979).

<sup>35</sup>F. J. Himpsel and D. E. Eastman, *Phys. Rev. B* **21**, 3207 (1980).

<sup>36</sup>W. Eberhardt and E. W. Plummer, *Phys. Rev. B* **21**, 3245 (1980).

<sup>37</sup>J. A. Knapp, F. J. Himpsel, and D. E. Eastman, *Phys. Rev. B* **19**, 4952 (1979).

<sup>38</sup>J. Stohr, P. S. Wehner, R. S. Williams, G. Apai, and D. A.

- Shirley, Phys. Rev. B **17**, 587 (1978).
- <sup>39</sup>D. E. Eastman, J. Vac. Sci. Technol. **17**, 492 (1980), and references therein.
- <sup>40</sup>T. C. Chiang, J. A. Knapp, M. Aono, and D. E. Eastman, Phys. Rev. B **21**, 3513 (1980).
- <sup>41</sup>T. Grandke, L. Ley, and M. Cardona, Phys. Rev. B **18**, 3847 (1978).
- <sup>42</sup>N. G. Stoffel, Phys. Rev. B **28**, 3306 (1983).
- <sup>43</sup>L. I. Johansson, A. Callenas, P. M. Stefan, A. Christensen, and K. Schwarz, Phys. Rev. B **24**, 1883 (1981).
- <sup>44</sup>J. H. Weaver, A. M. Bradshaw, J. F. van der Veen, F. J. Himpsel, D. E. Eastman, and C. Politis, Phys. Rev. B **22**, 4921 (1980).
- <sup>45</sup>J. Lindstrom, L. I. Johansson, A. Callenas, D. S. L. Law, and A. N. Christensen, Phys. Rev. B **35**, 7891 (1987).
- <sup>46</sup>C. H. Chen, W. Fabian, F. C. Brown, K. C. Woo, B. Davis, B. Delong, and A. H. Thompson, Phys. Rev. B **21**, 615 (1980).
- <sup>47</sup>W. Gopel, J. Pollmann, I. Ivanov, and B. Reihl, Phys. Rev. B **26**, 3144 (1982).
- <sup>48</sup>G. Zwicker and K. Jacobi, Solid State Commun. **54**, 701 (1985).
- <sup>49</sup>N. B. Brooks, D. S. L. Law, T. S. Padmore, D. R. Warburton, and G. Thornton, Solid State Commun. **57**, 473 (1986).
- <sup>50</sup>K. Siratori, S. Suga, M. Taniguchi, K. Soda, S. Kimura, and A. Yanase, J. Phys. Soc. Jpn. **55**, 690 (1986).
- <sup>51</sup>R. J. Lad and V. E. Henrich (unpublished).
- <sup>52</sup>N. V. Smith, in *Photoemission in Solids, Part I*, Vol. 26 of *Topics in Applied Physics*, edited by M. Cardona and L. Ley (Springer-Verlag, Berlin, 1978).
- <sup>53</sup>See, for example, G. D. Mahan, in *Electron and Ion Spectroscopy of Solids*, Vol. B32 of *NATO Advanced Study Institute*, edited by L. Fiermans, J. Vennik, and W. Dekeyser (Plenum, New York, 1978), p. 1; W. E. Spicer, *ibid.* p. 54.
- <sup>54</sup>E. O. Kane, Phys. Rev. Lett. **12**, 97 (1964).
- <sup>55</sup>J. Hermanson, Solid State Commun. **22**, 9 (1977).
- <sup>56</sup>B. D. Culity, *Elements of X-Ray Diffraction*, 2nd ed. (Addison-Wesley, Reading, MA, 1978), p. 504.
- <sup>57</sup>P. D. Dernier, J. Phys. Chem. Solids **31**, 2569 (1970).
- <sup>58</sup>J. C. Slater, *Quantum Theory of Molecules and Solids* (McGraw-Hill, New York, 1965), Vol. II, p. 418.
- <sup>59</sup>L. C. Davis, J. Appl. Phys. **59**, R25 (1986), and references therein.
- <sup>60</sup>E. Bertel, R. Stockbauer, and T. E. Madey, Phys. Rev. B **27**, 1939 (1983); E. Bertel, R. Stockbauer, R. L. Kurtz, D. E. Ramaker, and T. E. Madey, *ibid.* **31**, 5580 (1985).
- <sup>61</sup>R. D. Bringans and H. Hochst, Phys. Rev. B **30**, 5416 (1984).
- <sup>62</sup>P. A. P. Lindberg, L. I. Johansson, J. B. Lindstrom, and D. S. L. Law, Phys. Rev. B **36**, 939 (1987).
- <sup>63</sup>J. Barth, F. Gerken, and C. Kunz, Phys. Rev. B **31**, 2022 (1985).
- <sup>64</sup>S. Raaen and V. Murgai, Phys. Rev. B **36**, 887 (1987).
- <sup>65</sup>J. L. Dehmer, A. F. Starace, U. Fano, J. Sugar, and J. W. Cooper, Phys. Rev. Lett. **26**, 1521 (1971).
- <sup>66</sup>B. Reihl, N. Mårtensson, D. E. Eastman, A. J. Arko, and O. Vogt, Phys. Rev. B **26**, 1842 (1982).
- <sup>67</sup>A. J. Arko, D. D. Koelling, and B. Reihl, Phys. Rev. B **27**, 3955 (1983).
- <sup>68</sup>J. M. Mackay and V. E. Henrich, Surf. Sci. **137**, 463 (1987).
- <sup>69</sup>K. E. Smith and V. E. Henrich, Phys. Rev. B **32**, 5384 (1985).
- <sup>70</sup>K. E. Smith, Ph.D. thesis, Yale University, 1988.
- <sup>71</sup>R. L. Kurtz and V. E. Henrich, Phys. Rev. B **26**, 6682 (1982).
- <sup>72</sup>G. K. Wertheim and H. J. Guggenheim, Phys. Rev. B **22**, 4680 (1980).
- <sup>73</sup>D. K. G. deBoer, C. Haas, and G. A. Sawtsky, Phys. Rev. B **29**, 4401 (1984).
- <sup>74</sup>B. W. Veal and A. P. Paulikas, Phys. Rev. B **31**, 5399 (1985).
- <sup>75</sup>E. Sachar, Phys. Rev. B **31**, 4029 (1985); **34**, 5130 (1986).
- <sup>76</sup>F. J. Szalkowski, P. A. Bertrand, and G. A. Somorjai, Phys. Rev. B **9**, 3369 (1974).
- <sup>77</sup>V. E. Henrich, H. J. Zeiger, and G. Dresselhaus, in *Electrocatalysis on Non-Metallic Surfaces*, Natl. Bur. Stand. (U.S.) Spec. Publ. No. 455 (U.S. GPO, Washington, D.C., 1976), p. 133.

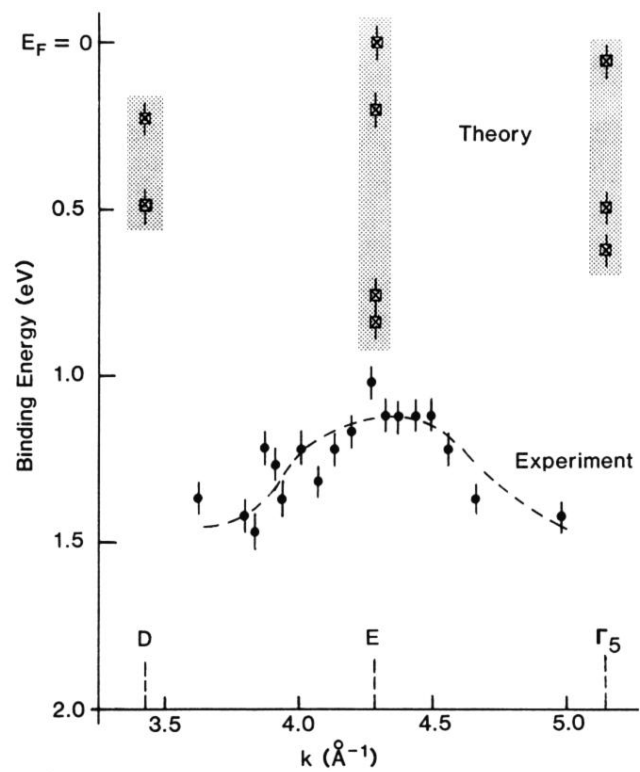


FIG. 10. Cation  $d$ -band dispersion in  $\text{V}_2\text{O}_3$ . Measured dispersions is indicated by  $\bullet$ . Theoretically predicted points from Ref. 10 are also shown. See text for details.

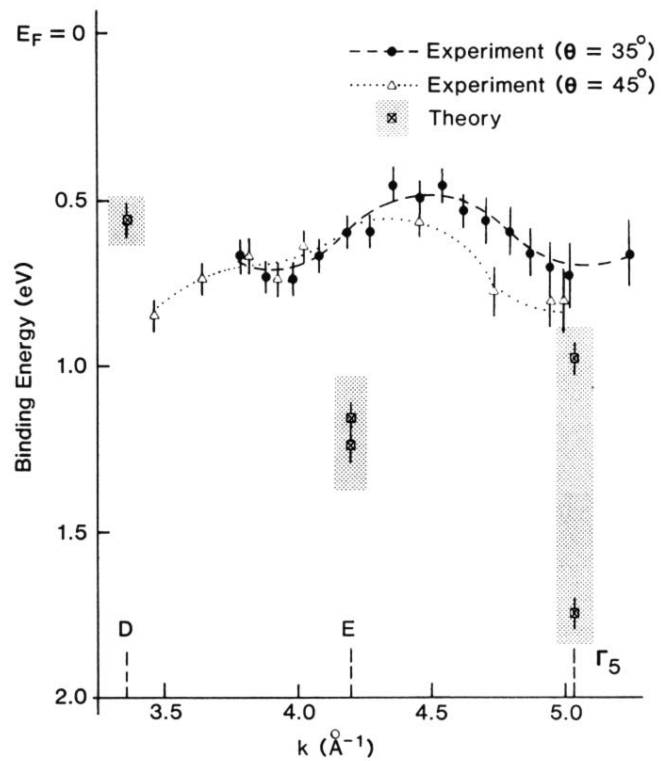


FIG. 9. Cation  $d$ -band dispersion in  $\text{Ti}_2\text{O}_3$ . Measured dispersions are indicated by  $\bullet$  and  $\triangle$ ; the lines shown are merely guides to the eye. Theoretically predicted points from Ref. 10 are also shown. See text for details.